Level structures of ^{96,97,98}Ru at high angular momentum

B. Kharraja, S. S. Ghugre,* and U. Garg
Department of Physics, University of Notre Dame, Notre Dame, Indiana 46556

R. V. F. Janssens, M. P. Carpenter, B. Crowell,† T. L. Khoo, T. Lauritsen, and D. Nisius
Physics Division, Argonne National Laboratory, Argonne, Illinois 60439

W. Reviol, W. F. Mueller,‡ and L. L. Riedinger
Department of Physics, University of Tennessee, Knoxville, Tennessee 37996

R. Kaczarowski
Soltan Institute for Nuclear Studies, 05-400 Swierk, Poland
(Received 24 July 1997)

The high-spin level structures of ^{96,97,98}Ru ($Z=44$) have been investigated using the ^{65}Cu(^{36}S, pxn)^{96,97,98}Ru ($x=4,3,2$) reactions. About 130 new transitions have been observed and unambiguously placed in the decay schemes of these nuclei. The level schemes have been extended up to spin $J\approx22-34\hbar$, and excitation energies $E_x\approx20-24$ MeV. Spherical shell model calculations have been performed and theoretical level energies compared with experimental values. Calculations using ^{88}Sr as the core give a reasonable agreement for the observed energy levels up to $J\leq16\hbar$ (the maximum angular momentum possible within this restricted model space). The higher angular momentum states are dominated by the $\nu(g_{9/2})^{-1}$ configuration, associated with breaking of the $N=50$ core. The experimental indications for this ''core breaking'' are (i) the observation of γ rays with energies $E_\gamma\approx2$ MeV at intermediate spins and (ii) the fragmentation of γ-ray intensity into a number of branches. A cascade of $E2$ transitions of nearly equal transition energies has been observed in ^{98}Ru after the core breaking ($J\geq16\hbar$), possibly manifesting vibrational behavior. [S0556-2813(98)00501-9]

PACS number(s): 27.60.+j, 23.20.Lv, 21.60.Cs

I. INTRODUCTION

Several experimental studies of Ru isotopes at moderate spins have been devoted to the search for the onset of collectivity near the $N=50$ closed shell [1–4]. These studies revealed interesting information on the low-spin structure of these nuclei. From the theoretical point of view, several models, such as the shell model [5], the vibrating core model [6], and the interacting boson model [7] have been used to describe the nature of the low-lying levels in these nuclei. Until recently, only limited information was available on the high-spin structures in these nuclei, making it impossible to extend the tests of these models to higher-angular-momentum states. With the advent of heavy-ion accelerators and Compton-suppressed Ge detector (CSGe) arrays, the experimental situation has improved and information is now available on the high spin states in nuclei in the $N\sim50$ region [8,9]. The low-lying states (up to $J^\pi=14^+$) of the nucleus ^{94}Ru ($N=50$) have been interpreted as being dominated by proton excitations within the $f_{5/2},p_{3/2},p_{1/2},g_{9/2}$ orbits [10]. Beyond that, levels up to spin $20\hbar$ were assumed to be dominated by the excitation of a single neutron across the $N=50$ shell closure, coupled to the protons in the fpg sub-

space. Furthermore, it was suggested that levels with spins greater than $J=22\hbar$ are dominated by the excitation of several neutrons across the $N=50$ shell gap [10]. For the low-lying states of ^{95}Ru ($N=51$) [11], the dominant proton and neutron configurations were $\pi(p_{1/2},g_{9/2})$ and $\nu(d_{5/2},s_{1/2})$; the higher-angular-momentum states were generated by the breaking of the neutron $N=50$ core in this case as well. On the other hand, collective degrees of freedom seem to play a dominant role in heavier Ru isotopes as the valence neutrons fill up the 50–82 subshell occupying, in particular, the shape-driving $h_{11/2}$ orbital. For example, collective excitations, band crossings, and quasiparticle alignments are now well established in ^{99}Ru ($N=55$) and ^{100}Ru ($N=56$) [12] and the level energies indicate that a transition towards band termination might occur at the top of the yrast cascade of ^{100}Ru [12].

Located between these two modes of excitations, i.e., between single particle behavior ($N\leq51$) and collective behavior ($N\geq55$), the nuclei ^{96,97,98}Ru are very attractive candidates to search for the onset of collectivity above the $N=50$ closed shell. Theoretical calculations have predicted γ softness and shape coexistence persisting to high spins in these nuclei. Recent total Routhian surface (TRS) calculations of Wyss *et al.* [13] predict the existence of deformed neutron configurations with negative parity, associated with the $\nu(h_{11/2})$ orbital, in $^{96-98}$Ru. These configurations correspond to a near-prolate shape ($\gamma\sim0°$), but the expected deformations are small ($\beta_2<0.13$) and the local minima in the TRS's are rather shallow. However, these deformed minima

---

can be stabilized by the addition of aligned $g_{9/2}$ protons to the configuration. Also, a half-filled $\nu(g_{9/2})$ orbit was found to be deformation-driving in the $A \sim 80$ region [14] and the Ru nuclei ($Z=44$) correspond to the half-filled $\pi(g_{9/2})$ shell. A detailed investigation of these nuclei, therefore, could help explore the deformation-driving characteristics of a half-filled $g_{9/2}$ proton orbit.

II. EXPERIMENTAL METHODS

The γ decay of the excited states in ^{96,97,98}Ru has been investigated using the early implementation phase of the Gammasphere spectrometer [15] which at that time comprised 36 large ($\geqslant 70\%$ relative efficiency) CSGe detectors. The experiment was carried out at the 88 in. Cyclotron of the Ernest O. Lawrence Berkeley National Laboratory. The ^{96,97,98}Ru nuclei were populated via the ^{65}Cu(^{36}S, pxn) ($x=4,3,2$) reactions at a bombarding energy of 142 MeV. Two stacked, self-supporting target foils of thickness ~ 0.5 mg/cm^2 each were used. A data set of approximately 400 million events, each requiring at least a triple prompt coincidence between CSGe detectors, was recorded during the measurement; the final data consisted of approximately 73% triple-, 19% quadruple-, and 4% quintuple-coincidence events. The most strongly populated nuclei were the $^{96-98}$Ru isotopes (corresponding to 16.3, 20.4, and 18.3 % of the total γ-ray flux, respectively) reported herein. Several other reactions channels, such as those leading to ^{94,95,96}Tc (8.2, 12.2, and 4.1 %), ^{94,95}Mo (8.0 and 4.3 %), and ^{97,98}Rh (4.7 and 3.5 %) final nuclei, were also populated in the experiment with significant intensities; these nuclei are the subject of separate investigations [16].

The observation of very weak γ transitions, of the order of 10^{-3} in relative intensity when compared to the most intense transition, has been made possible by the combination of the high statistics and the superior efficiency for threefold and higher coincidence events provided by Gammasphere. Two symmetrized E_γ-E_γ-E_γ cubes, in the Radford [17] and Kuehner [18] formats, have been used during the data analysis. The Radford-format cube was analyzed using the RADWARE analysis package [19], which uses a generalized background subtraction procedure [20] for extracting double-gated coincidence spectra from the cube. In the Kuehner-format cube, these spectra were obtained using the FUL background subtraction algorithm [21]. Many new transitions have been observed and placed in the decay schemes of these nuclei. The selectivity afforded by ''double gating'' and the presence of many crossover transitions in the level schemes of ^{96,97}Ru provide many checks of the placement and ordering of transitions, and serve to bolster confidence in the correctness of the proposed level schemes. The same holds true for the multipolarity assignments which are based primarily on the intensity ratios extracted using angle-sorted matrices. In our procedure, coincidence gates are placed on spectra of the forward-angle (32° and 37°) detectors, and the γ rays measured at 90° and at backward angles (143° and 147°) are sorted along the two axes of the matrices. Although such directional correlation ratios, $R = I_\gamma(\text{backward})/I_\gamma(90°)$, have their limitations (for example, the stretched quadrupole transitions cannot be distinguished from $\Delta I=0$ dipoles or certain $\Delta I=1$ transitions),

reliable spin assignments can be made, nonetheless, by comparing the ratios of the new γ lines with those of previously known γ rays whose multipolarity is already firmly established. Supporting evidence for the spin assignments is provided, in many cases, by the presence of crossover transitions observed in these nuclei. The highest spins assigned in the present work are somewhat less certain since crosschecks from parallel cascades are not available. Tables I–III list all γ rays assigned to ^{96}Ru, ^{97}Ru, and ^{98}Ru, respectively, along with their intensities, the intensity-ratios R (where available), and the suggested placements in the level schemes.

III. EXPERIMENTAL RESULTS

A. Level scheme of ^{96}Ru

The level scheme of ^{96}Ru, as deduced from this work, is shown in Fig. 1 and a typical double-gated γ-ray coincidence spectrum is shown in Fig. 2. The high sensitivity of the Gammasphere array has enabled the observation and placement of about 40 new transitions.

The previously known level scheme of ^{96}Ru consisted of two independent sequences (1 and 2 in Fig. 1) of opposite parities [9]. The positive-parity sequence (sequence 1) was known up to spin (22^+). The change made with respect to the high-spin levels reported in Ref. [9] is that the 600-keV transition placed in this sequence [connecting the (20^+) and (18^+) levels] is not observed in our data; we do observe a 595-keV dipole transition, however, which has been placed at the top of this sequence. The previously known (18^+) level is now fed directly by the 1043-keV transition and two new dipole transitions of 748 and 595 keV. Also, the 447-keV transition placed parallel to the 112- (110 keV in Ref. [9]) and 337-keV transitions is now located higher in the scheme, below the 822-keV transition, and links the (12^+) and (11^+) levels. An $M1$ character has been assigned to the new dipole transitions in $^{96-98}$Ru, based on mass systematics [11,22] and shell model comparisons (see below). The DCO ratios of these transitions indicate values higher than the values generally associated with pure $E1$ transitions, and are similar to those for $M1$ transitions with strong $E2$ admixtures. Above $J=16\hbar$, sequence 1 is fragmented into several cascades with the same highest-observed spin ($J=22\hbar$) for each of these.

Several γ transitions of energies around 2 MeV (1744, 1746, 1765, 1817, 2058, 2111, and 2289 keV) feeding the (16^+) level have been observed in the present work. Their significance is discussed later.

The main negative-parity branch (sequence 2) has been extended to the (23^-) level. The new transitions in this sequence are of energies 601 and 1609 keV, respectively. The sequence of γ rays of energies 781, 747, 1000, and 584 keV, feeding the $9^{(-)}$ state in Ref. [9], has been slightly modified and extended to higher spins by the observation of the 227-, 1429-, 678-, and 499-keV transitions (sequence 3 in Fig. 1). These two cascades (sequences 2 and 3) are linked by four crossover, dipole transitions of 1155, 476, 265, and 218 keV. The important change with respect to the high-spin levels reported in Ref. [9] is that the 781-keV transition in the negative-parity sequence has been placed at a higher spin and excitation energy [deexciting the (17^-) level].

TABLE I. Energies, initial and final spins, relative intensities, and directional correlation ratios R (as defined in the text) for ^{96}Ru.

E_γ (keV)[a]	$J_i \to J_f$ [b]	I_γ [c]	R [d]	E_γ (keV)[a]	$J_i \to J_f$ [b]	I_γ [c]	R [d]
112.1	$(10^+) \to 10^+$	2.0 (4)		801.2	$8^+ \to 6^+$	67.2	2.1 (2)
150.2	$(14^+) \to (13^+)$	1.5 (4)		822.0	$(13^+) \to (12^+)$	2.0 (6)	1.5 (3)
217.7	$13^- \to (12^-)$	6.0 (1.0)	1.6 (2)	831.6	$2^+ \to 0^+$	100.0	1.8 (1)
222.7	$(9^+) \to 8^+$	1.0 (4)	1.5 (3)	849.2	$11^- \to 9^-$	50.0	
227.0	$(21^-) \to (19^-)$	1.2 (3)		850.2	$(20^+) \to (18^+)$	1.0 (3)	2.1 (3)
237.3	$\to 16^+$	$\leqslant 1$		867.3	$10^+ \to 8^+$	57.0	2.2 (1)
265.1	$(11^-) \to 10^-$	1.0 (3)	1.5 (3)	893.9	$(12^+) \to (10^+)$	1.1 (4)	
292.7	$(12^+) \to (12^+)$	1.0 (3)		952.9	$13^- \to 11^-$	36.1	2.0 (2)
328.2	$\to 16^+$	$\leqslant 1$		973.4	$17^+ \to (16^+)$	1.0 (5)	
337.2	$(11^+) \to (10^+)$	1.2 (4)		977.2	$(19^+) \to (18^+)$	$\leqslant 1$	
446.7	$(12^+) \to (11^+)$	1.4 (4)		1000.3	$12^- \to 10^-$	19.0	1.9 (2)
447.0	$(14^+) \to (13^+)$	1.0 (4)		1002.1	$9^- \to 8^+$	1.0 (3)	
475.6	$15^- \to 14^-$	17.6	1.6 (2)	1004.4	$15^- \to 13^-$	26.9	2.1 (2)
499.4	$16^- \to 14^-$	17.8	2.2 (2)	1043.3	$20^+ \to 18^+$	2.0 (6)	1.8 (3)
501.0	$(18^+) \to 18^-$	1.0 (5)		1071.1	$5^- \to 4^+$	47.0	1.3 (3)
528.8	$14^- \to 13^-$	15.0	1.6 (2)	1093.2	$17^+ \to (16^+)$	1.0 (4)	
584.1	$10^- \to 9^-$	28.0	1.6 (2)	1134.0	$22^+ \to 20^+$	1.3 (3)	2.0 (3)
595.4	$(22^+) \to (21^+)$	1.0 (2)		1155.0	$19^- \to 18^-$	10.0	
597.2	$14^- \to (14^+)$	5.0 (8)	3.1 (3)	1197.4	$17^- \to 15^-$	26.0	1.9 (2)
601.3	$(12^+) \to 10^+$	47.0	1.8 (2)	1229.1	$18^+ \to 17^+$	$\leqslant 1$	
601.4	$(18^+) \to (17^+)$	1.0 (4)	1.5 (3)	1262.3	$14^+ \to 12^+$	25.0	2.0 (2)
601.0	$(21^-) \to (19^-)$	10.1	1.9 (2)	1299.1	$(18^-) \to 17^-$	1.0 (5)	
632.1	$6^+ \to 4^+$	85.0	1.9 (2)	1382.4	$(22^+) \to 20^+$	$\leqslant 1$	
660.4	$9^- \to 7^-$	63.0	2.0 (2)	1429.2	$(19^-) \to 18^-$	1.0 (3)	1.6 (3)
677.9	$18^- \to 17^-$	16.8	1.5 (3)	1440.4	$19^- \to 17^-$	5.0 (1.0)	1.9 (3)
685.1	$4^+ \to 2^+$	96.0	1.9 (2)	1447.0	$(16^+) \to (14^+)$	1.0 (5)	
703.9	$7^- \to 5^-$	58.0	2.0 (2)	1459.3	$18^- \to 16^-$	1.0 (6)	
735.2	$12^- \to 11^-$	8.4	1.5 (2)	1609	$(23^-) \to 21^-$	1.0 (4)	2.1 (3)
746.5	$14^- \to 12^-$	5.0	2.0 (3)	1744	$16^+ \to 14^+$	1.0 (4)	
748.3	$21^+ \to 20^+$	1.8 (4)	1.6 (3)	1746	$(17^+) \to (16^+)$	1.0 (4)	
751.2	$(20^+) \to (18^+)$	1.0 (5)		1765	$18^+ \to 16^+$	3.5 (8)	1.8 (3)
761.1	$(16^+) \to (14^+)$	12.0	2.2 (2)	1817	$(22^+) \to (20^+)$	$\leqslant 1$	
779.4	$9^- \to (9^+)$	1.1 (6)		2058	$(17^+) \to (16^+)$	1.0 (2)	
781.4	$17^- \to 16^-$	21.1	1.5 (2)	2111	$(22^+) \to (20^+)$	$\leqslant 1$	
781.2	$(18^+) \to (17^+)$	$\leqslant 1$		2289	$(18^+) \to (16^+)$	1.0 (2)	
780.8	$(18^+) \to (16^+)$	1.0 (5)					

[a]The transitions of energies $\leqslant 1500$ keV are known to ~ 0.4 keV; for the higher energies the uncertainties are ~ 1 keV.

[b]The J^π of the levels for which the ratio R could not be extracted and which are not fixed by other interband transitions are given in parentheses.

[c]Except where stated, the uncertainties in intensities are less than 10%.

[d]A blank is kept for all the transitions for which no ratio R could be obtained.

The positive-parity and negative-parity cascades are connected at low spins by three crossover transitions (1002, 223, and 779 keV), and at high spins by the 597-, 1459-, and 501-keV γ rays. The $7^{(-)}$ level appears to feed the positive-parity sequence at spin 8^+, but the "linking" transitions could not be identified.

B. Level scheme of ^{97}Ru

Figure 3 illustrates a typical double-gated γ-ray spectrum for ^{97}Ru and the level scheme obtained for this nucleus is displayed in Fig. 4. This was the most intensely populated nucleus in this work and about 50 new transitions have been observed and unambiguously placed in the level scheme, which has been extended up to $J > 53/2\hbar$ and $E_x \approx 18$ MeV. Most of the intensity feeds through the level sequence (sequence 1) shown on the left of the level scheme. In general, there is a good agreement with the results obtained previously [9]; however, some discrepancies have been noted. The major change compared to Ref. [9] is the observation of an 876-keV $M1$ transition linking the levels $(35/2^+)$ and $(33/2^+)$. Above this transition, the main positive-parity sequence splits into two parallel cascades. Another fragmentation of γ-decay strength occurs $4\hbar$ higher. Also, as in the case of ^{96}Ru, many new γ rays with energies around 2 MeV

TABLE II. Energies, initial and final spins, relative intensities, and directional correlation ratios R (as defined in the text) for ^{97}Ru.

E_γ (keV)[a]	$J_i \to J_f$ [b]	I_γ [c]	R [d]	E_γ (keV)[a]	$J_i \to J_f$ [b]	I_γ [c]	R [d]
155.1	$(19/2^+) \to (17/2^+)$	3.0 (5)	1.5 (3)	875.9	$(35/2^+) \to 33/2^+$	7.0	1.6 (2)
193.4	$21/2^+ \to 17/2^+$	40.0	2.0 (2)	879.3	$(9/2^+) \to (5/2^+)$	68.0	1.8 (2)
207.1	$(51/2^+) \to (49/2^+)$	4.0 (7)	1.6 (2)	882.1	$(47/2^+) \to (43/2^+)$	1.0 (3)	
216.0	$\to 39/2^+$	1.0 (5)		915.6	$(19/2^+) \to 15/2^+$	21.0	2.1 (2)
217.7	$(19/2^+) \to 17/2^+$	4.2 (6)	1.6 (2)	917.4	$(47/2^+) \to (45/2^+)$	2.0 (7)	1.5 (3)
230.1	[e]	$\leqslant 1\%$		933.4	$25/2^+ \to 21/2^+$	22.0	2.0 (2)
267.2	$33/2^+ \to (31/2^+)$	6.0 (1.0)	1.5 (2)	945.1	$(43/2^+) \to (39/2^+)$	1.0 (5)	
306.7	$(23/2^+) \to 21/2^+$	2.0 (4)	1.6 (3)	947.4	$(13/2^+) \to (9/2^+)$	22.0	1.9 (2)
316.7	$\to (51/2^+)$	1.0 (3)		949.9	$(23/2^+) \to (19/2^+)$	8.8	2.1 (2)
320.4	$11/2^+ \to 9/2^+$	15.0	1.5 (2)	960.7	$(49/2^+) \to (47/2^+)$	4.0 (8)	1.5 (3)
330.0	$(41/2^+) \to (39/2^+)$	1.0 (4)		1000.2	$(11/2^-) \to (9/2^+)$	8.0	1.3 (2)
343.5	$(31/2^+) \to (29/2^+)$	2.0 (5)		1029.1	[f]	2.0 (1.0)	
376.5	$(31/2^+) \to 29/2^+$	2.0 (6)		1028.0	$(31/2^-) \to (27/2^-)$	1.0 (4)	
422.1	$7/2^+ \to 5/2^+$	100.0	1.5 (1)	1040.2	$(47/2^+) \to (43/2^+)$	1.0 (5)	
430.1	$(53/2^+) \to (51/2^+)$	4.0 (7)	1.6 (3)	1044.3	$(27/2^+) \to (23/2^+)$	13.0	1.9 (2)
457.2	$9/2^+ \to 7/2^+$	9.0	1.6 (2)	1062.3	$29/2^+ \to 25/2^+$	10.0	1.9 (2)
468.1	$29/2^+ \to 27/2^+$	13.0	1.6 (2)	1079.7	$(43/2^+) \to (39/2^+)$	1.0 (4)	
491.0	$(39/2^+) \to (37/2^+)$	2.1 (5)		1109.4	$(41/2^+) \to (39/2^+)$	14.0	1.5 (2)
501.1	$(29/2^+) \to 27/2^+$	2.0 (5)		1143.1	$(45/2^+) \to (41/2^+)$	1.0 (5)	
525.0	$(47/2^+) \to 45/2^+$	$\leqslant 1$		1164.4	$(47/2^+) \to (45/2^+)$	6.0 (1.0)	1.6 (3)
594.2	$27/2^+ \to 25/2^+$	13.0	1.6 (2)	1198.1	$(49/2^+) \to (47/2^+)$	6.0 (1.2)	1.5 (3)
632.5	$(35/2^+) \to (31/2^+)$	7.0	2.1 (2)	1204.4	$(51/2^+) \to (49/2^+)$	6.0 (1.0)	1.5 (3)
642.1	$(37/2^+) \to (35/2^+)$	16.0	1.5 (2)	1230.1	$\to (53/2^+)$	5.0 (9)	
643.2	$(21/2^+) \to (19/2^+)$	2.0 (6)	1.6 (3)	1270.1	$(39/2^+) \to (37/2^+)$	3.0 (8)	1.6 (3)
642.6	$(27/2^+) \to (23/2^+)$	15.0	1.9 (2)	1275.4	$(45/2^+) \to (41/2^+)$	8.0	2.2 (2)
643.7	$33/2^+ \to 29/2^+$	23.0	1.8 (2)	1341.2	$(51/2^+) \to (49/2^+)$	1.0 (5)	
648.2	$15/2^+ \to 11/2^+$	89.0	2.0 (2)	1388.3	$(49/2^+) \to (47/2^+)$	4.0	
673.3	$(19/2^-) \to (15/2^-)$	4.0 (9)	2.1 (2)	1391.0	$(39/2^+) \to (35/2^+)$	16.0	2.1 (2)
674.3	$(15/2^-) \to (11/2^-)$	3.0 (1.0)	1.8 (3)	1419.2	$(47/2^+) \to (45/2^+)$	1.0	
695.0	$(53/2^+) \to (51/2^+)$	1.0 (2)		1457.3	$(53/2^+) \to (51/2^+)$	1.0	
698.2	$(39/2^+) \to (35/2^+)$	6.0	1.9 (2)	1479.1	$(51/2^+) \to (49/2^+)$	1.0	
699.9	$17/2^+ \to 15/2^+$	68.0	1.6 (2)	1481.2	$(31/2^+) \to (27/2^+)$	7.0	2.2 (3)
716.9	$(23/2^-) \to (19/2^-)$	3.0 (7)	2.0 (3)	1523	[g]	$\leqslant 1$	
721.1	$17/2^+ \to (13/2^+)$	1.0 (4)		1567	[g]	$\leqslant 1$	
727.1	$(15/2^-) \to (13/2^+)$	1.0 (4)		1601	$(41/2^+) \to (37/2^+)$	17.0	1.9 (2)
736.7	$(45/2^+) \to (43/2^+)$	15.0	1.5 (2)	1620	[f]	$\leqslant 1$	
753.3	$(27/2^-) \to (23/2^-)$	2.0 (6)	1.9 (3)	1626	$(47/2^+) \to (45/2^+)$	1.0	
772.7	$(13/2^+) \to (9/2^+)$	16.0	1.8 (2)	1638	$(43/2^+) \to (41/2^+)$	6.0	
777.6	$11/2^+ \to 7/2^+$	88.0	2.1 (1)	1653	$(47/2^+) \to (43/2^+)$	1.0	
796.1	$(31/2^-) \to (27/2^-)$	1.0 (4)		1795	$\to (53/2^+)$	1.0	
801.7	$(47/2^+) \to (43/2^+)$	4.0 (9)		1845	$(41/2^+) \to (37/2^+)$	1.0	
823.2	$(35/2^-) \to (31/2^-)$	1.0 (3)		1879	$(49/2^+) \to (45/2^+)$	1.0	
830.4	$(43/2^+) \to (39/2^+)$	16.0	1.8 (2)	1883	[h]	1.0	
842.0	$(47/2^+) \to (43/2^+)$	1.0 (5)		1901	$\to (47/2^+)$	$\leqslant 1$	
844.6	$(31/2^+) \to 27/2^+$	15.0	1.9 (2)	2083	[i]	$\leqslant 1$	
855.4	$(17/2^+) \to (13/2^+)$	7.1	1.8 (3)	2153	$\to (51/2^+)$	1.0	
862.4	$(23/2^+) \to (19/2^+)$	17.0	2.0 (2)				

[a]The transitions of energies $\leqslant 1500$ keV are known to ~ 0.4 keV; for the higher energies the uncertainties are ~ 1 keV.

[b]The J^π of the levels for which the ratio R could not be extracted and which are not fixed by other interband transitions are given in parentheses.

[c]Except where stated, the uncertainties in intensities are less than 10%.

[d]A blank is kept for all the transitions for which no ratio R could be obtained.

[e]The 230-keV transition feeds the 216-keV transition.

[f]The 1029- and 1620-keV transitions feed the 1230-keV transition.

[g]The 1523- and 1567-keV transitions feed the 1620-keV transition.

[h]The 1883-keV transition feeds the 1204-keV transition.

[i]The 2088-keV transition feeds the 1883-keV transition.

TABLE III. Energies, initial and final spins, relative intensities, and directional correlation ratios R (as defined in the text) for ^{98}Ru.

E_γ (keV)[a]	$J_i \rightarrow J_f$ [b]	I_γ [c]	R [d]	E_γ (keV)[a]	$J_i \rightarrow J_f$ [b]	I_γ [c]	R [d]
277.2	$(26^+) \rightarrow (24^+)$	≤ 1		1107.2	$(27^-) \rightarrow (25^-)$	1.0 (4)	
399.4	$(25^+) \rightarrow (24^+)$	10.0	1.6 (2)	1223.2	$(25^-) \rightarrow (24^-)$	≤ 1	
406.9	$(23^-) \rightarrow (22^-)$	1.5 (3)		1230.4	$(15^-) \rightarrow (13^-)$	10.0	1.9 (3)
456.3	$(29^+) \rightarrow (28^+)$	≤ 1		1281.1	$(27^+) \rightarrow (26^+)$	1.0 (4)	
500.1	$(29^+) \rightarrow (28^+)$	≤ 1		1287.3	$(17^-) \rightarrow (15^-)$	12.5	2.2 (3)
652.9	$2^+ \rightarrow 0^+$	100.0	1.9 (2)	1403.7	$(19^-) \rightarrow (17^-)$	5.7 (8)	2.1 (3)
725.7	$(18^+) \rightarrow (16^+)$	22.0	2.0 (3)	1442.9	$(28^+) \rightarrow (27^+)$	1.0 (3)	
746.2	$4^+ \rightarrow 2^+$	81.0	1.8 (2)	1465.3	$(28^+) \rightarrow (26^+)$	≤ 1	
800.3	$(11^-) \rightarrow (9^-)$	5.5 (9)	1.9 (3)	1475.0	$(26^+) \rightarrow (24^+)$	15.0	2.1 (2)
810.9	$(9^-) \rightarrow (7^-)$	2.5 (1.0)		1481.6	$(24^+) \rightarrow (22^+)$	21.0	1.9 (2)
821.3	$(12^+) \rightarrow (10^+)$	23.0	2.1 (2)	1509	$(29^+) \rightarrow (27^+)$	≤ 1	
825.3	$6^+ \rightarrow 4^+$	57.0	2.0 (2)	1738	$(30^+) \rightarrow (28^+)$	5.2 (8)	2.1 (3)
826.1	$(20^+) \rightarrow (18^+)$	19.0	1.9 (2)	1773	$(26^-) \rightarrow (25^-)$	≤ 1	
848.4	$(10^+) \rightarrow 8^+$	31.0	2.1 (2)	1789	$(34^+) \rightarrow (32^+)$	1.3 (6)	
875.2	$(9^-) \rightarrow 8^+$	1.0 (4)		1827	$(30^+) \rightarrow (28^+)$	1.0 (5)	
876.7	$(22^+) \rightarrow (20^+)$	28.0	2.0 (2)	1863	$(30^+) \rightarrow (28^+)$	1.0 (5)	
888.8	$(26^+) \rightarrow (25^+)$	≤ 1		1941	$(28^+) \rightarrow (27^+)$	≤ 1	
904.1	$8^+ \rightarrow 6^+$	26.0	1.9 (2)	1970	$(26^+) \rightarrow (24^+)$	1.3 (5)	
905.0	$(22^-) \rightarrow (21^-)$	1.5 (4)		1985	$(24^-) \rightarrow (22^-)$	1.1 (5)	
912.1	$(21^-) \rightarrow (20^-)$	3.0 (8)	1.5 (3)	2055	$(28^+) \rightarrow (26^+)$	1.0 (5)	
969.4	$(7^-) \rightarrow 6^+$	7.1	1.3 (3)	2065	$(30^+) \rightarrow (28^+)$	1.2 (5)	
989.8	$(25^-) \rightarrow (24^-)$	1.0 (6)		2085	$(27^+) \rightarrow (25^+)$	1.3 (5)	
995.1	$(13^-) \rightarrow (11^-)$	14.0	2.0 (2)	2160	$(30^+) \rightarrow (28^+)$	≤ 1	
995.4	$(20^-) \rightarrow (19^-)$	4.1 (9)		2125	$(28^+) \rightarrow (26^+)$	1.0 (5)	
1017.2	$(24^-) \rightarrow (23^-)$	1.2 (5)		2181	$(38^+) \rightarrow (36^+)$	1.0 (5)	
1024.3	$(28^+) \rightarrow (26^+)$	3.6 (8)	2.1 (3)	2192	$(32^+) \rightarrow (30^+)$	1.0 (5)	
1032.2	$(14^+) \rightarrow (12^+)$	30.0	1.9 (2)	2215	$(36^+) \rightarrow (34^+)$	1.0 (5)	
1050.1	$(27^-) \rightarrow (25^-)$	1.0 (2)		2223	$(32^+) \rightarrow (30^+)$	1.0 (5)	
1070.1	$(16^+) \rightarrow (14^+)$	34.0	2.0 (3)	2227	$(29^-) \rightarrow (27^-)$	≤ 1	
1075.6	$(26^+) \rightarrow (25^+)$	9.5	1.6 (2)				

[a]The transitions of energies $\leq$ 1500 keV are known to $\sim$ 0.4 keV; for the higher energies the uncertainties are $\sim$ 1 keV.
[b]The J^π of the levels for which the ratio R could not be extracted and which are not fixed by other interband transitions are given in parentheses.
[c]Except where stated, the uncertainties in intensities are less than 10%.
[d]A blank is kept for all the transitions for which no ratio R could be obtained.

have been observed at higher spins, i.e., at about $J \geq 37/2\hbar$. This common feature of the level schemes will be discussed below.

In the second positive-parity sequence of the level scheme (sequence 2), the earlier work [9] had placed the 155-keV γ ray below the 855-keV transition; the present data indicate the opposite ordering, based on intensity considerations. Furthermore, there is no indication in the present data for the 882-keV γ ray which was placed above the 773-keV transition in Ref. [9]. An 882-keV transition is present, but it has now been placed at higher spin and excitation energy [i.e., above the $(43/2^+)$ level]. This sequence has now been extended to $(47/2^+)$ due to the observation of the 1080- and 842-keV transitions. Two additional cascades of two transitions each [(945-, 1040-keV) and (216-, 230-keV)] were observed parallel with the uppermost part of this sequence. At low spins, two coincident dipole transitions (307 and 643 keV) are found to be parallel to the 950-keV $E2$ transition.

A $\Delta J = 2$ cascade built on the $(11/2^-)$ state, consisting of three transitions (717, 673, and 674 keV) had been previ-

ously reported [3]. This cascade (sequence 3) has been extended by three new $E2$ transitions (753, 796, and 823 keV). The highest spin reached in this band is $(35/2^-)$. The intensity of this band is very weak compared to the positive-parity bands: $\sim$ 3% of the total intensity as obtained from the 422- and 879-keV γ rays. The $(11/2^-)$ state is linked to the positive-parity branch via the 1000-keV $E1$ transition to the $9/2^+$ level and the $(15/2^-)$ level feeds the $(13/2^+)$ level through the 727-keV transition.

There are indications of linking transitions between sequence 1 and the negative-parity sequence at high spins in that the 1143- and 1845-keV transitions depopulating the $(45/2^+)$ level appear to feed the negative-parity sequence at spin $(31/2^-)$. Unfortunately, the linking transitions (presumably very weak) could not be observed in this experiment.

C. Level scheme of ^{98}Ru

A representative coincidence spectrum obtained for ^{98}Ru is given in Fig. 5 and the level scheme for this nucleus is shown in Fig. 6. Above the 8^+ state, and parallel to the main
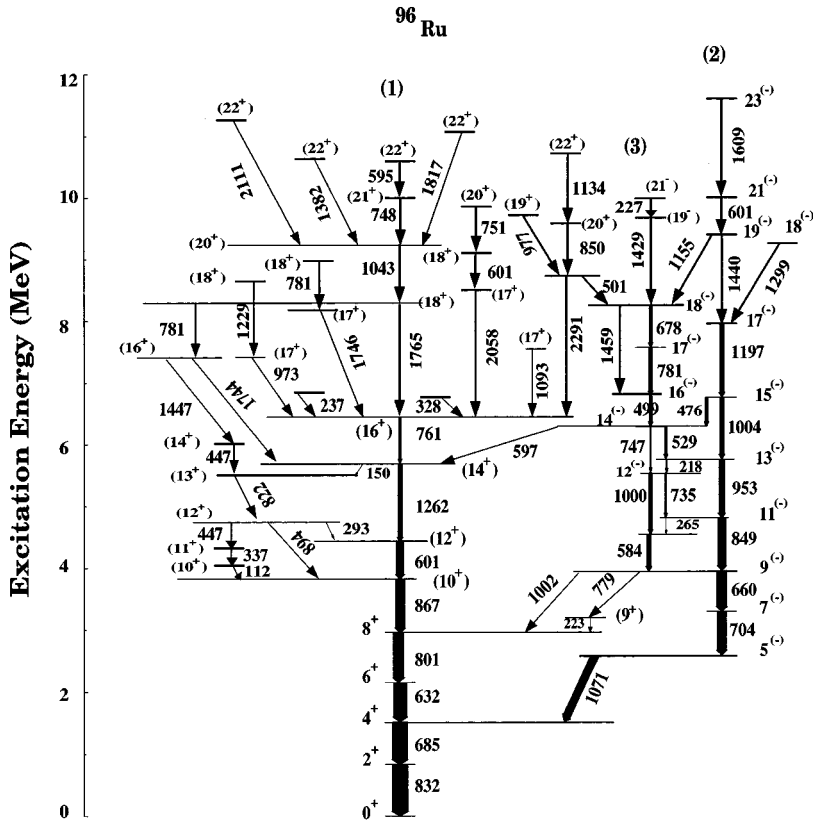
FIG. 1. Level scheme of ^{96}Ru obtained from the present work. The energies are labeled in keV. The widths of the arrows are approximately equal to the relative intensities of the observed γ transitions.

level structure (sequence 1), a regular cascade of quadrupole transitions is observed up to spin (19^-). The γ-ray energies of these $E2$ transitions increase monotonically with spin between (9^-) and (19^-). This sequence (marked 2 in Fig. 6) is then followed by a number of dipole transitions, of energies 995, 912, 905, 407, 1017, and 990 keV. A total of ten new transitions have been placed in sequence 2, extending it up to

$E_x \approx 18$ MeV. This cascade is fragmented at high spins, and among the new transitions are three $E_\gamma \approx 2$ MeV γ rays (1773, 1985, and 2227 keV).

In a previous investigation of ^{98}Ru, several transitions had been reported at low spin using the ^{98}Mo$(\alpha, 4n\gamma)$ reaction [23]. Some of these transitions belong to nonyrast sequences which are not populated in heavy-ion-induced re-
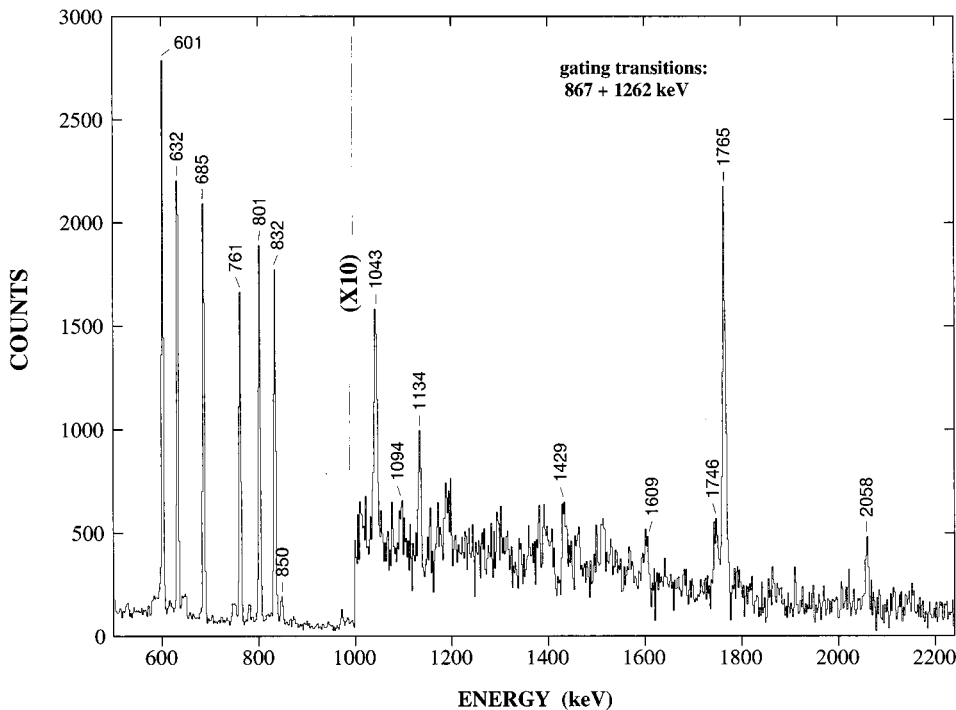
FIG. 2. Representative double-gated coincidence γ spectrum for ^{96}Ru. The transition energies are marked to within $\pm$ 1 keV.
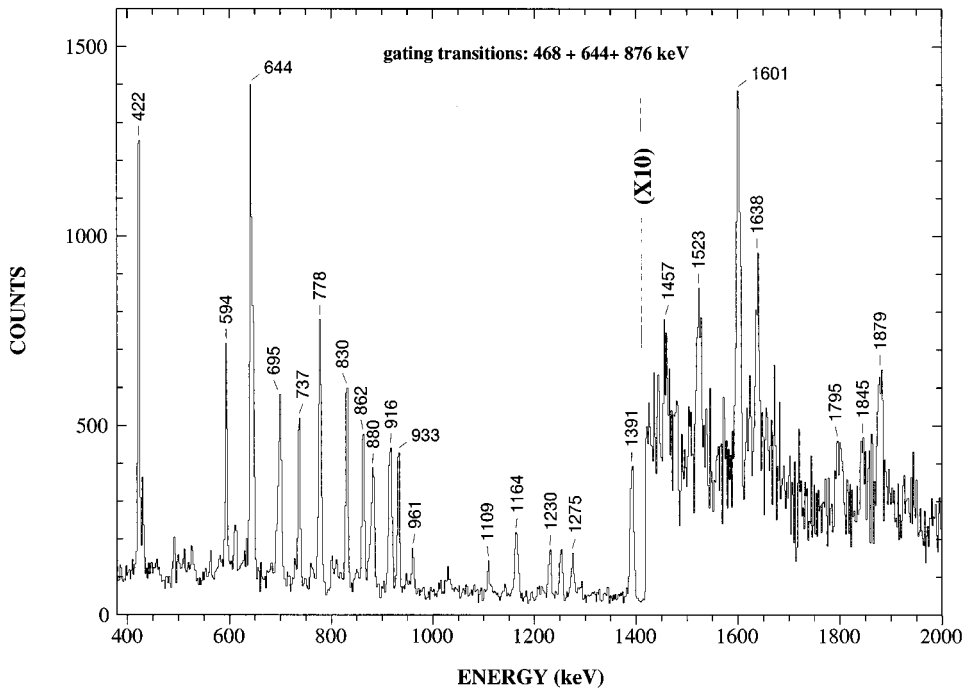
FIG. 3. Representative double-gated coincidence γ spectrum for ^{97}Ru. The transition energies are marked to within $\pm$ 1 keV.

actions, and could not be observed in the present work. The placement of a few transitions has been revised as compared to the earlier results. The most important change is that an opposite-parity assignment has been proposed in Ref. [23] for all states above 8^+, and for some low-spin states. For example, an $E2$ character has been assigned to the 969-keV line, while the present data indicate a dipole (most likely an $E1$) character. However, the authors of Ref. [23] have stated that in most cases no unique spin and parity assignment could be made on the basis of strong arguments. They also reported many discrepancies in reproducing the branching ratios, using IBA calculations, for the states above the 8^+ level. In addition, a study of the nonyrast states of ^{98}Ru via the ^{97}Mo(α, $2n\gamma$) reaction [24] also had disagreements with Ref. [23], in both spin and transition assignments.

The present data indicate also certain discrepancies with respect to the latest investigation of this nucleus [9]. There, two transitions of 644 and 1148 keV were proposed as connecting the $7^- \rightarrow 5^- \rightarrow 4^+$ levels; these have not been observed in the present work. Transitions of these energies are present in ^{95}Tc [16] and could have been erroneously attributed to ^{98}Ru earlier. Furthermore, the placement of the 1017- and 1773-keV (1016 and 1771 in Ref. [9]) transitions in sequence 2 has been revised, based primarily on coincidence and intensity considerations; these γ rays are now placed at higher spins and excitation energies. A negative parity is proposed for this sequence on the basis of (i) comparisons with the shell-model calculations presented below and (ii) energy-level systematics in this mass region (see discussion below).

The previously known positive-parity sequence (sequence 1) included 12 $E2$ transitions decaying from the (24^+) level to the ground state [9]. The ordering of γ-ray transitions of 848 and 821 keV in this sequence has been changed, based on the observed intensity pattern. A total of 23 new transitions have been identified and placed in this sequence. Above spin $J=24\hbar$, a fragmentation of strength occurs, as is

the case in ^{96,97}Ru. The most intense branch is fed by two dipole transitions of 399 and 1076 keV, followed by a new sequence of $E2$ transitions. These transitions, in order of increasing spin, are of 1738-, 2192-, 1789-, 2215-, and 2181-keV energy. All of them are very weak and it is possible that the ordering of the 2181- and 2215-keV transitions could be reversed. A second fragmentation appears at the (28^+) level and several new cascades appear in parallel with sequence 1. A total of 14 transitions of ≈ 2 MeV energy have been identified at high spins. Overall, the level scheme has been extended up to $J=38\hbar$ and excitation energy $E_x \approx 24$ MeV, the highest spin and excitation energy observed in this experiment, and represents a gain of $14\hbar$ in spin and ≈ 14 MeV in excitation energy in comparison with the previous work [9].

The positive- and negative-parity branches appear to be linked at low and high spins. However, the linking transitions could not be identified from the coincidence spectra.

IV. DISCUSSION

As mentioned above, the low-lying levels in $N \geqslant 50$ nuclei are well described by spherical shell model calculations with ^{88}Sr as the inert core and a $[\pi(p_{1/2},g_{9/2});\nu(d_{5/2},s_{1/2})]$ valence space [25]. Such a small configuration space is inadequate to describe the higher-angular momentum states in these nuclei. For example, using the above basis, the maximum angular momentum possible for nuclei with $N \geqslant 50$ is typically around $16\hbar$. To obtain a more appropriate description of the observed high-spin level sequences, large-basis shell model calculations are necessary. These higher-angular-momentum states could be dominated by (i) the excitation of the neutrons into higher orbitals, such as $\nu(h_{11/2},g_{7/2})$, (ii) the excitation of the $g_{9/2}$ neutrons across the $N=50$ core into the next major oscillator shell, or (iii) most likely, a combination of these two processes. In an earlier study of the high-spin states in ^{94}Tc [22], a comparison of the experimental excitation energies with the shell-
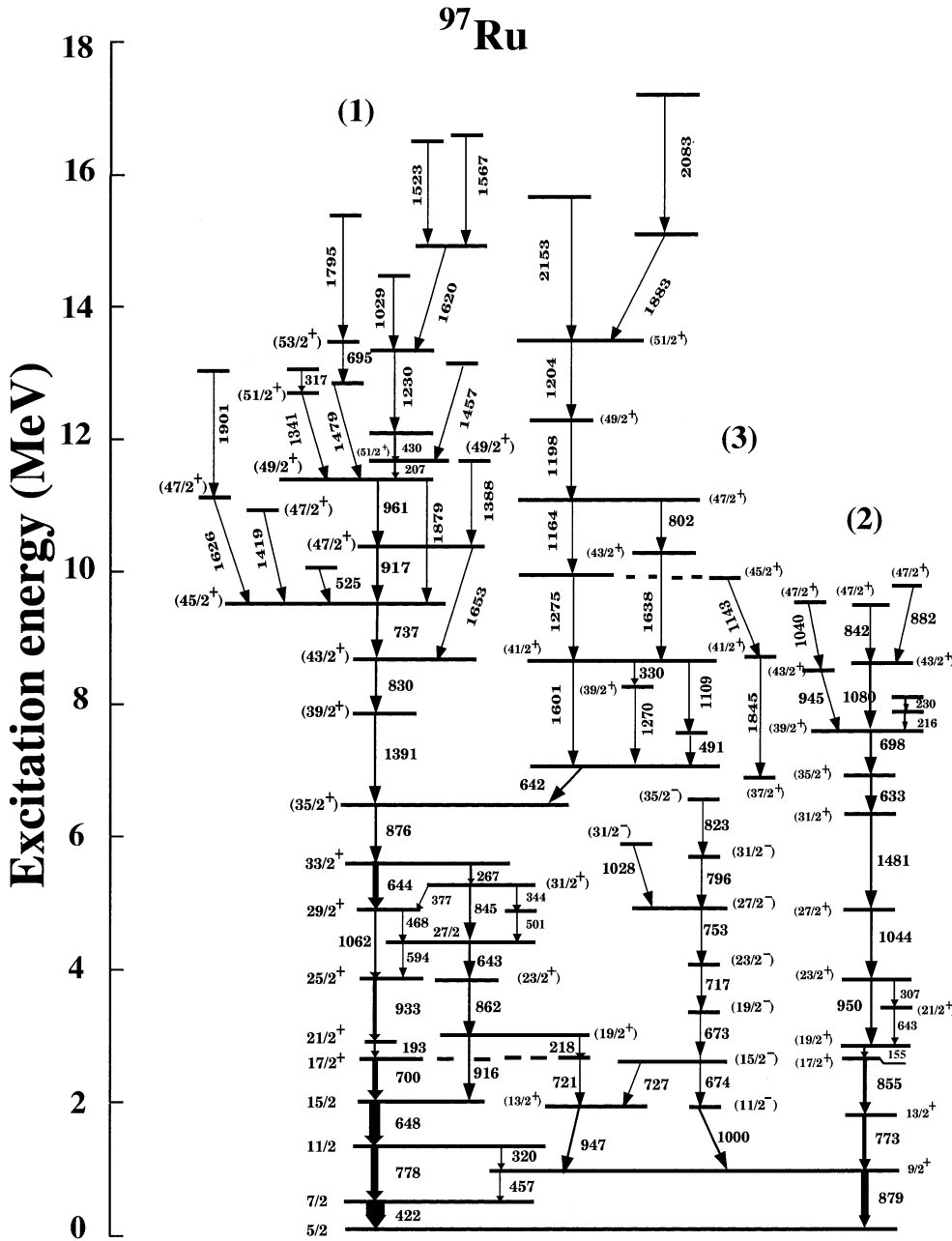
FIG. 4. Level scheme of ^{97}Ru obtained from the present work. The energies are labeled in keV. The widths of the arrows are approximately equal to the relative intensities of the observed γ transitions.

model calculations using ^{88}Sr, ^{66}Ni, and ^{56}Ni as the core has been reported. It was noted that the inclusion of the $\nu(f_{5/2})$ orbitals in the core (^{56}Ni) resulted in a somewhat better agreement with the experimental energy levels. It would appear, therefore, that to adequately describe the observed higher-angular-momentum states in these nuclei, shell model calculations would need to be performed using a model space comprising the $\pi(f_{5/2}, p_{3/2}, p_{1/2}, g_{9/2})$ and $\nu(f_{5/2}, p_{3/2}, p_{1/2}, g_{9/2}, d_{5/2}, g_{7/2}, h_{11/2})$ valence orbitals outside a ^{56}Ni inert core. Such unrestricted, large-basis calculations are not feasible at present due to computational limitations and a truncation scheme has to be devised. The details of one such truncation procedure are given in Ref. [10]. In the next sections, we will present results of shell-model calculations using both small and large configuration spaces for ^{96}Ru. For ^{97,98}Ru, results of the shell-model calculations using only the

small model space, as well as those from a weak-coupling scheme will be presented.

A. ^{96}Ru: Single particle configurations

Shell model calculations for ^{96}Ru were performed within the model space named GL in the code OXBASH [26]. This model space encompasses the $\pi(p_{1/2}, g_{9/2})$ and $\nu(d_{5/2}, s_{1/2})$ orbits outside the ^{88}Sr inert core. The two-body matrix elements were taken from the work of Gloeckner [27] and include no contribution from core excitation.

Figure 7 compares the experimental excitation energies with the calculations. Within the restricted model space used, the maximum angular momentum possible for ^{96}Ru, with six valence protons and two valence neutrons outside ^{88}Sr, is $J = 16\hbar$. The experimental results and the shell model calculations are in good agreement up to spin $16\hbar$ for the positive-parity sequence (Fig. 7) and up to spin $15\hbar$ for the negative-
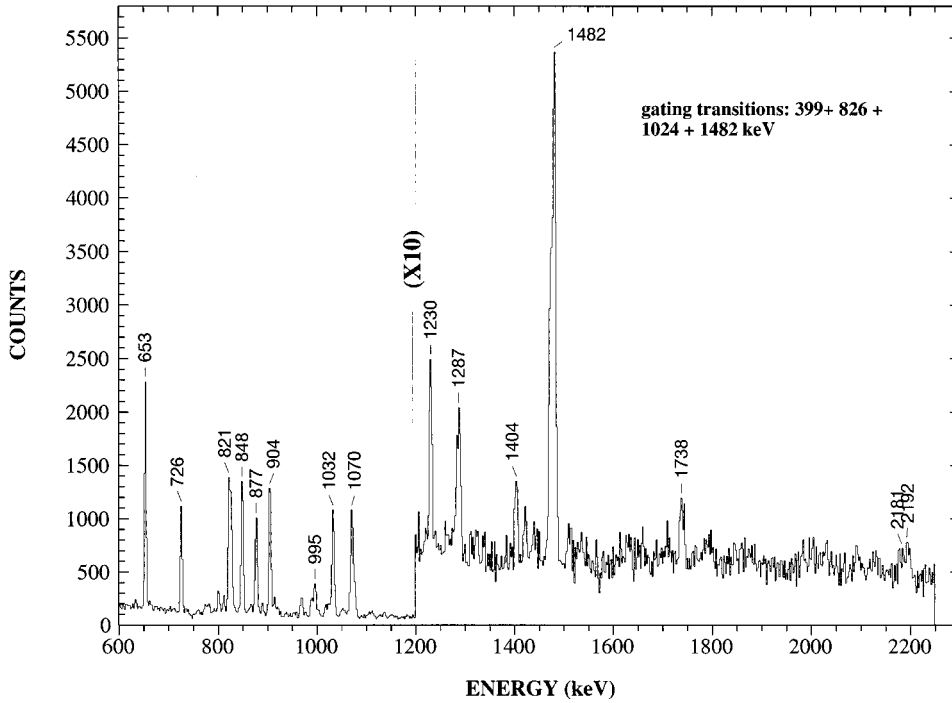
FIG. 5. Representative double-gated coincidence γ spectrum for ^{98}Ru. The transition energies are marked to within $\pm$ 1 keV.

parity sequence. The excitation energy predicted by the shell model code for the 16^- state is markedly higher than the experimental value. This discrepancy could be a result of significant contributions to this level from configurations other than $\pi(p_{1/2},g_{9/2})\otimes\nu(d_{5/2},s_{1/2})$.

The level schemes of $^{96-98}$Ru show the presence of γ rays with energies of the order of $E_\gamma\approx2$ MeV at and above the level $J=16\hbar$. These transitions are indicative of the breaking of the $N=50$ core. This conclusion is based on the following observations: (i) no such high-energy transitions exist at the lower spins, (ii) several ~2-MeV transitions appear in parallel with each other—such fragmentation of intensity suggests a profound change in structure whereby several competing excitation pathways become available, (iii) these transitions appear at spins that are consistent with the maximum spins possible from the available orbitals without breaking the core, and (iv) these spins and excitation energies are in agreement with the shell-model predictions for core breaking. A similar feature had been reported previously in the $A\sim150$ region: for example, in the nucleus ^{150}Dy, two parallel cascades were observed and were attributed to the simultaneous breaking of the $Z=64$ and $N=82$ cores [28]. Further, Roth *et al.* [8] and Ghugre *et al.* [11] have observed a similar feature in ^{95}Rh and ^{95}Ru as well.

Because of this core breaking, the higher-angular-momentum states are likely to be dominated by the excitation of $g_{9/2}$ neutrons across the $N=50$ magic shell [10], and could involve the

$$\pi(p_{1/2},g_{9/2})\otimes\nu[(g_{9/2})^{-1},(d_{5/2})^{+1}]$$

$$\pi(p_{1/2},g_{9/2})\otimes\nu[(g_{9/2})^{-1},(g_{7/2})^{+1}]$$

$$\pi(p_{1/2},g_{9/2})\otimes\nu[(g_{9/2})^{-1},(h_{11/2})^{+1}]$$

configurations. Hence, shell model calculations were performed using an enlarged configuration space which encompassed eight proton orbitals $[\pi(f_{5/2},p_{3/2},p_{1/2},g_{9/2},g_{7/2},d_{5/2},d_{3/2},s_{1/2})]$ and nine neutron orbitals $[\nu(f_{5/2},p_{3/2},p_{1/2},g_{9/2},g_{7/2},d_{5/2},d_{3/2},s_{1/2},h_{11/2})]$ outside an inert ^{56}Ni core. This model space is named SNE in the OXBASH code [26]. A combination of schematic and experimental two-body matrix elements, provided for in OXBASH, was used. Due to computational limitations, the large model space was internally truncated by considering only the most dominant configurations for a given angular momentum state. The details of this truncation procedure are described in Ref. [10]. For levels with $J\leqslant16\hbar$, no neutron excitations were allowed across the $N=50$ magic shell and the $\pi(f_{5/2},p_{3/2})$ orbitals were completely occupied (i.e., proton excitations were allowed only within the $p_{1/2},g_{9/2}$ orbitals). For the higher-angular momentum states, calculations were performed by incorporating the excitation of a single $g_{9/2}$ neutron across the $N=50$ core into the next major oscillator shell (i.e., the $[(g_{9/2})^{-1},(d_{5/2})^{+1}]$, $[(g_{9/2})^{-1},(s_{1/2})^{+1}]$, and $[(g_{9/2})^{-1},(g_{7/2})^{+1}]$ configurations). Due to computational limitations, calculations incorporating the $[\nu(g_{9/2})^{-1},(h_{11/2})^{+1}]$ configuration could not be carried out.

Figure 8 shows the comparison between the experimental excitation energies and the "extended basis" shell model calculations. Once again there is a reasonable agreement between the experimental and theoretical excitation energies for the low-lying levels ($J\approx16\hbar$). The inclusion of the $\nu(h_{11/2})$ orbital results in a better agreement for the $J=16^-$ state, which reinforces the interpretation that this state is indeed dominated by the occupation of the $\nu(h_{11/2})$ orbital. However, there is a distinct discrepancy between the shell-model predictions and the experimentally observed excitation energies for the higher-angular momentum states [dominated by the $\nu(g_{9/2})^{-1}$ configurations]: the calculated energy
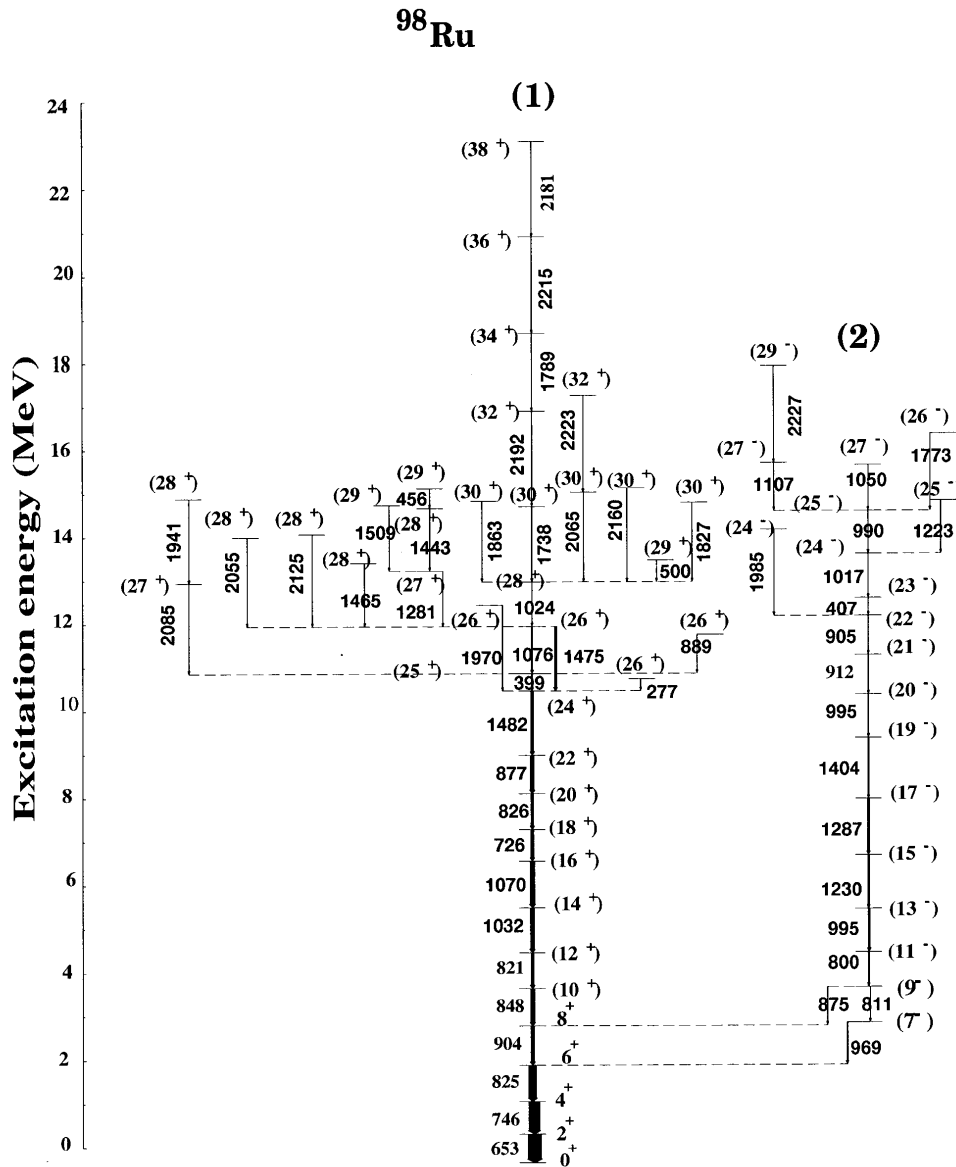
^{98}Ru

(1)

(2)

FIG. 6. Level scheme of ^{98}Ru obtained from the present work. The energies are labeled in keV. The widths of the arrows are approximately equal to the relative intensities of the observed γ transitions.

gap between the lower states and those that appear after breaking the $N=50$ shell is much larger than seen in the data. This discrepancy could possibly be attributed to either (a) the truncation scheme used or (b) the effective interactions used. The effect of the former could, perhaps, be simulated empirically by normalizing the theoretical excitation energy of one of the high-lying states (say, $J=17\hbar$) to the experimental value (such a normalization procedure has previously been adopted by Kabadiyski and co-workers for the case of ^{90}Mo [29]). Clearly, the ''post-normalization'' agreement between the theoretical and experimental energy levels would, then, be rather good. As for (b), the experimental effective interactions used in the calculations were derived by fitting the low-spin data. However, in the absence of any previous experimental information on the states involving the breaking of the $N=50$ core, these values have so far not been tested for higher spins. It is hoped that the present data will lead to the development of better effective interactions in this region, especially for those states involving the $\nu(g_{9/2})^{-1}$ configurations.

It is also possible that the negative-parity states are domi-

nated by other configurations than those considered above, such as the excitation of neutrons within the ($g_{7/2}, d_{5/2}, d_{3/2}, s_{1/2}, h_{11/2}$) orbits coupled to proton excitations within fpg subshell. Unfortunately, these configurations could not be incorporated in the calculations, due to the large dimensionality of the m subspace when high-j orbitals such as $h_{11/2}$ are involved. Nevertheless, the shell-model calculations involving both these model spaces indicate qualitatively the single-particle nature of the observed level sequences in ^{96}Ru: particle excitations within the $\pi(p_{1/2}, g_{9/2}); \nu(d_{5/2}, s_{1/2}, h_{11/2})$ dominate the low-lying levels ($J \leqslant 16\hbar$); the higher angular-momentum states appear to be dominated by the excitation of a $g_{9/2}$ neutron across the $N=50$ magic shell.

Another noteworthy result of these calculations pertains to the negative-parity sequence observed in ^{96}Ru, consisting of six stretched $E2$ transitions and feeding into the 7^- state. These states are well reproduced by the shell model calculations, although the regularity of the energy spacings, and the relatively strong $E2$ transitions, are quite suggestive of collective degrees of freedom [9].
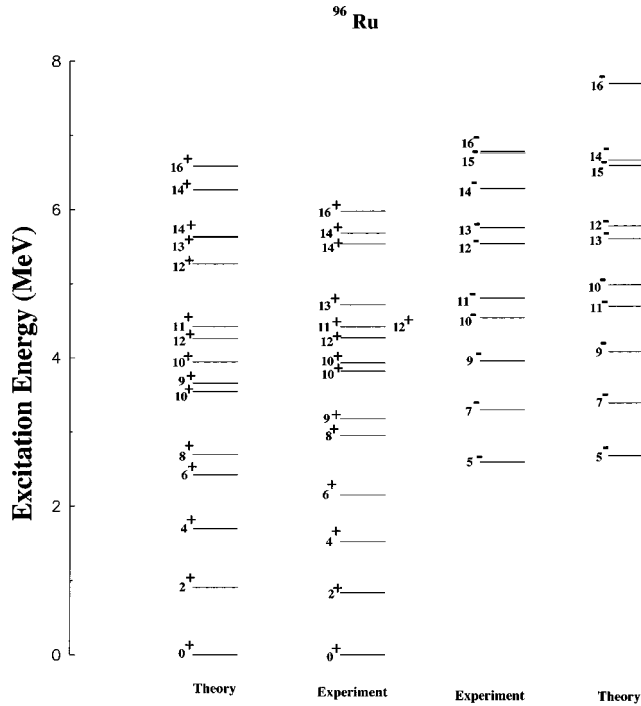
FIG. 7. Comparison of the observed states up to spin $J=16\hbar$ in ^{96}Ru with spherical shell model calculations, using the small configuration space GL (see text for details).

B. ^{97}Ru and ^{98}Ru: Shell model description and beyond

As stated above, the nuclei ^{97,98}Ru lie in a region where a transition from spherical, single particle behavior to collective phenomena is quite likely to occur.

In a previous attempt at understanding the nature of ^{98}Ru, IBA calculations were performed for the low-lying levels (up to spin 10^+). Such calculations have led to the conclusion that ^{98}Ru can be described by the IBA-1 model (in its vibrational limit) with good results up to spin 8^+, beyond which the experimental excitation energies begin to deviate from the calculated values [23]. The authors of Ref. [24] have suggested another explanation, using the surface-delta residual interaction in a two-quasiparticle-plus rotor model. Skouras *et al.* [5] have already demonstrated that in this transitional region, various approaches, such as the shell model and the particle-rotor model give similar results, and the energy level systematics are insufficient to arrive at any definite conclusions regarding the underlying microscopic structure, highlighting the need for more complete spectroscopic information.

The success of the shell model calculations at low and moderate spins in ^{96}Ru makes an extension to ^{97,98}Ru imperative. Shell model calculations for these nuclei were first performed using the GL model space described above. Figures 9 and 10 show the comparison between the experimental excitation energies for ^{97}Ru and ^{98}Ru, respectively, and the shell model predictions up to $J\approx17\hbar$, the maximum angular momentum possible within this restricted model space. As seen from the figures there is a reasonable agreement between the theoretical and experimental values, up to the highest spins. However, the agreement between the theoretical and experimental excitation energies for the $J=7/2^+$, $11/2^+$, $15/2^+$, $27/2^+$, and $31/2^+$ levels in
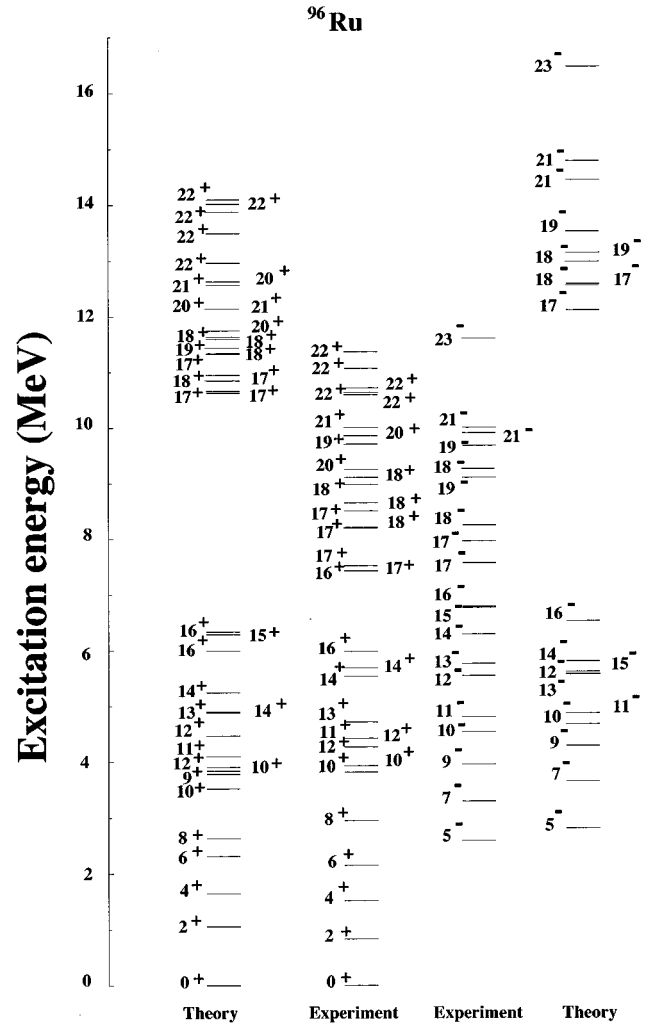

FIG. 8. Comparison of the observed states for the higher spins in ^{96}Ru with the spherical shell model calculations, using the model space SNE (see text for details).

^{97}Ru is markedly poorer than for other states (Fig. 9). Again, this may be attributed to the contribution from other configurations such as $\nu(g_{7/2},h_{11/2})$ which were not included in the calculations.

The weak-coupling model has also been quite successful in interpreting the level sequences in the $N\approx50$ nuclei. The levels of the "$N+1$" [e.g., ^{97}Ru(J)] nucleus could be obtained by coupling the $d_{5/2}$ or $g_{7/2}$ neutron orbitals to the "N" [^{96}Ru(J)] core. The level structures of Nb, Tc, and Rh isotopes were well described by this model [16,30]. Figure 11 illustrates the weak-coupling scheme for ^{97}Ru. Levels up to $J=49/2^+$ and $35/2^-$ can be qualitatively explained in this weak-coupling approximation. The levels in ^{97}Ru dominated by the $[^{96}$Ru(J)$\otimes\nu(g_{7/2})]$ coupling would lie about 420 keV higher in excitation energy than the corresponding levels in ^{96}Ru. This is attributed to the fact that the $\nu(g_{7/2})$ orbital has an excitation energy of about 420 keV with respect to the $\nu(d_{5/2})$ orbital (as seen from the excitation energy of 422 keV for the $7/2^+$ level). The coupling gives good agreement for the excitation energies of the $J=7/2^+,11/2^+,15/2^+,$ $27/2^+,31/2^+$ levels (which could not be explained satisfactorily by the shell model), implying that these levels are in-
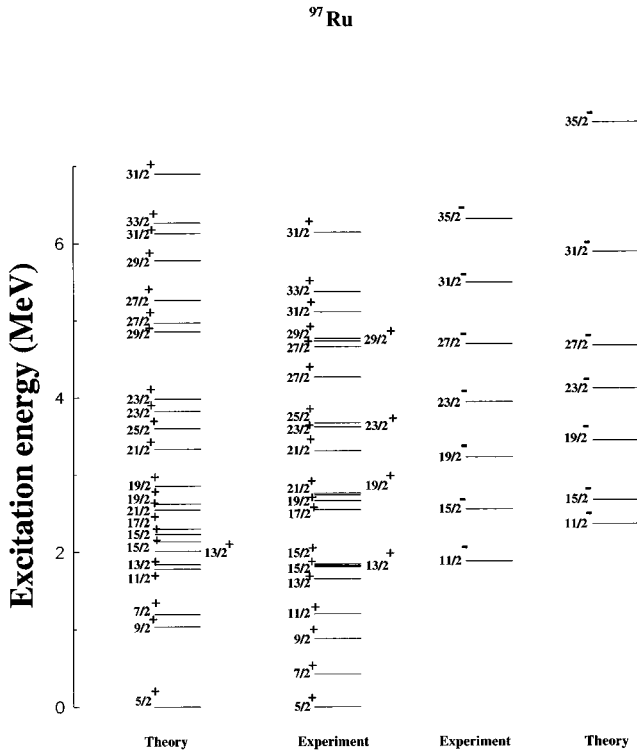
FIG. 9. Comparison of the observed excitation energies and the spherical shell model predictions within the GL model space up to spin $J \approx 16\hbar$ for ^{97}Ru.

FIG. 10. Comparison of the observed states up to spin $J = 17\hbar$ in ^{98}Ru with the spherical shell model calculations, using the restricted model space GL.

deed dominated by the $\nu(g_{7/2})$ orbitals which were not incorporated in the shell model calculations. However, similar excitation energies were obtained for the $J = 19/2^+$, $23/2^+$ levels in both the shell model, and the weak-coupling scheme using the $[^{96}$Ru$(J) \otimes \nu(d_{5/2})]$ and $[^{96}$Ru$(J) \otimes \nu(g_{7/2})]$ configurations. Also, the $E2$ ''band-like'' sequence in ^{97}Ru is well reproduced within both models.

As discussed above, the breaking of the $N = 50$ core in ^{96}Ru occurs above $J = 16^+$, as evidenced in the level scheme by the presence of γ rays with $E_\gamma \approx 2$ MeV and the onset of several parallel pathways. A similar feature can be seen in ^{97}Ru above $J = 37/2^+$ $[^{96}$Ru$(J = 16) \otimes \nu(d_{5/2})]$, suggesting that the higher-angular-momentum states in ^{97}Ru are, again, dominated by the excitation of a $\nu(g_{9/2})$ neutron across the $N = 50$ magic shell. Thus, the shell model calculations and the weak-coupling scheme qualitatively suggest single-particle nature for the observed levels up to high spins and excitation energies ($J \approx 22\hbar$, $E_x \approx 12$ MeV) in ^{97}Ru.

As seen from Fig. 10, levels up to $J = 16^+$ and 17^- in ^{98}Ru are well reproduced within the shell model calculations (using the restricted GL model space). In this case also, the shell model calculations reproduce the sequence of $E2$ transitions observed in the negative-parity part of the level scheme. This lends support to the negative-parity assignment for this ''band.'' The weak-coupling scheme $[^{98}$Ru$(J') = ^{97}$Ru$(J) \otimes \nu(d_{5/2})]$ is also reasonably successful in reproducing the observed positive-parity sequences up to $J = 16^+$, as illustrated in Fig. 12. However, this scheme cannot reproduce the level sequences above this state (which corresponds
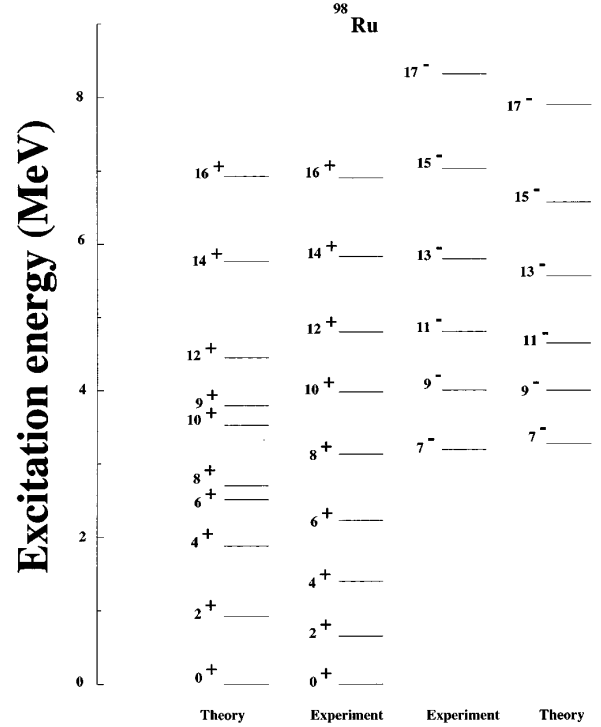
to the $J = 37/2^+$ state in ^{97}Ru) where the breaking of the $N = 50$ core is expected. This difference between ^{97}Ru and ^{98}Ru could be because of major contributions from other intrinsic configurations [such as $\nu(h_{11/2})$] for the higher-angular momentum states in ^{98}Ru, before the breaking of the core. The weak-coupling approximation could not be extended to the negative-parity band in ^{98}Ru, due to the fact that experimental information on the corresponding states in ^{97}Ru is not available.

The nucleus ^{98}Ru has a ''band'' built on the 9^- state, consisting of five $E2$ transitions with energies monotonically increasing with spin, followed by dipole transitions with irregular level spacings and a fragmentation of the intensity into different branches. Within the rotational model, this would typically be an indication of a ''band termination.'' As stated before, the ''band'' in ^{96}Ru exhibits almost the same general trend and the ''band termination'' occurs at the same spin (19^-) in both nuclei.

A weak $\Delta J = 2$ ''band,'' consisting of six $E2$ transitions, and built on the $11/2^-$ state, is observed in ^{97}Ru as well. This also is suggestive of the onset of collectivity and could be interpreted as a ''decoupled'' band built on the $h_{11/2}$ quasineutron state [3]. Similar $\Delta J = 2$ bands also have been observed in ^{99,101,103}Ru [12]; however, the band observed in ^{97}Ru is found to be much weaker than that in the heavier odd Ru isotopes.

This observation of bandlike characteristics brings forth the need for a more detailed study of the intrinsic structure of these levels. As pointed out earlier, these bandlike cascades in ^{96,98}Ru can be reproduced rather well in the framework of the shell model and also in the weak-coupling calculations.
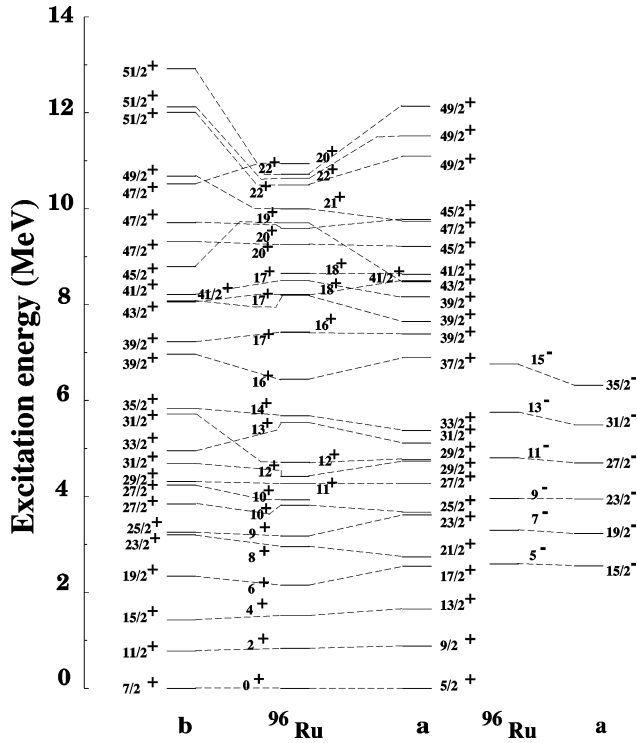
FIG. 11. Comparison of the energy levels in ^{96}Ru and ^{97}Ru assuming the: (a) $[^{97}\text{Ru}(J')=^{96}\text{Ru}(J)\otimes\nu(d_{5/2})]$ and (b) $[^{97}\text{Ru}(J')=^{96}\text{Ru}(J)\otimes\nu(f_{7/2})]$ stretched configurations. The levels corresponding to the configuration (b) have been plotted after substracting 422 keV from their excitation energy [the excitation energy of the $\nu(g_{7/2})$ orbit with respect of the $\nu(d_{5/2})$ orbit. See text for details].

FIG. 12. Comparison of the positive-parity levels in ^{97}Ru and ^{98}Ru assuming the weak-coupling of a $\nu(d_{5/2})$ neutron to the ^{97}Ru core $[^{97}\text{Ru}(J)+\nu(d_{5/2})=^{98}\text{Ru}(J')]$.

Lifetime measurements have been undertaken to further elucidate the true nature of these $E2$ cascades, and will be reported in a separate publication [31].

An intriguing aspect of the observed level structure in ^{98}Ru is the presence of a cascade of $E2$ transitions with energies $E_\gamma\approx 2$ MeV linking the very high spin ($J\gtrsim 28\hbar$) yrast states (see Fig. 6). This cascade of energies 1738, 2192, 1789, 2215, and 2181 keV is built on the (28^+) state, i.e., it occurs after the core breaking. In spherical nuclei, harmonic vibrational motion results in an excitation spectrum consisting of equally spaced degenerate phonon multiplets. Based on the observed level spacings, this band could be described as "vibrationlike." Incidentally, a similar "quasivibrational" cascade has been observed previously in ^{154}Ho, a nucleus located near the region of the onset of collectivity in the rare-earth regime. It was interpreted as indicative of a transition to soft triaxial shapes and of an increasing γ deformation at high spins [32].

V. SUMMARY

Extensive level schemes have been established for ^{96,97,98}Ru from data obtained with the early implementation Gammasphere array. A total of about 130 new γ transitions have been identified in these nuclei and, as a result, their level structures have been extended to high spins and excitation energies ($J\approx 22\hbar$, $E_x\approx 12$ MeV). Shell model calculations within the small configuration space using ^{88}Sr as the
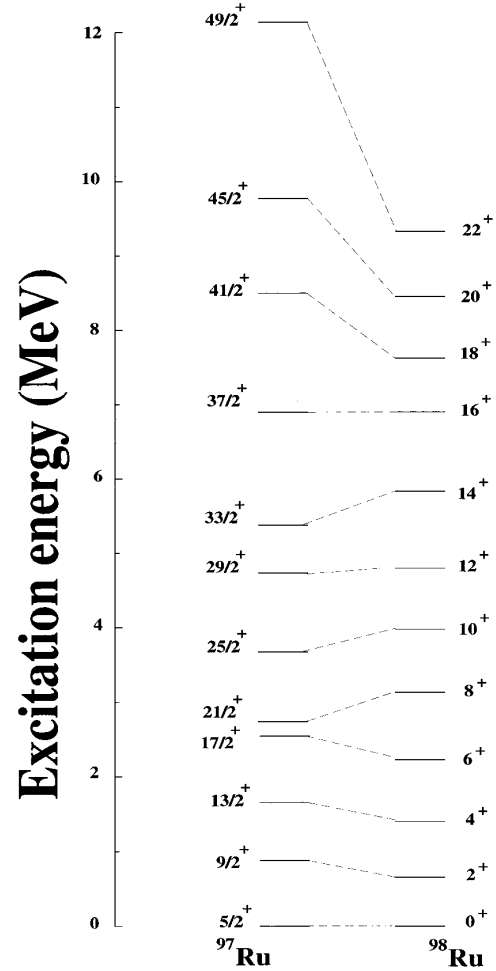
core agree reasonably well with the experimental energy levels up to $J\approx 16\hbar$ (the maximum angular momentum possible within this restricted space). The use of a larger configuration space shows that the higher-angular-momentum states are dominated by the excitation of a $g_{9/2}$ neutron across the $N=50$ magic shell. The observation of γ rays with $E_\gamma\approx 2$ MeV, and the associated fragmentation of the γ-ray flux into many competing pathways, provide a clear experimental signature for the breaking of the $N=50$ core. The core-breaking picture is also supported qualitatively by the shell-model calculations and by the weak-coupling scheme. The observed level structures of these nuclei exhibit single-particle nature even at the highest spins and excitation energies. Several cascades of $E2$ transitions of approximately equal energies ($E_\gamma\approx 2$ MeV) appear after the breaking of the $N=50$ core in ^{98}Ru. These cascades are suggestive of a "vibrational" character.

---

[1] C.M. Lederer, J.M. Jaklevic, and J.M. Hollander, Nucl. Phys. **A169**, 489 (1971).

[2] A. Goswami, M. Saha, S. Bhattacharya, B. Dasmahapatra, P. Basu, P. Bhattacharya, M.L. Chatterjee, P. Banerjee, and S. Sen, Phys. Rev. C **42**, 1367 (1990).

[3] P. Chowdhury, B.A. Brown, U. Garg, R.D. McKeown, T.P. Sjoreen, and D.B. Fossan, Phys. Rev. C **32**, 1238 (1985).

[4] G. Kajrys, J. Dubuc, P. Larivière, S. Pilotte, W. Del Bianco, and S. Monaro, Phys. Rev. C **34**, 1629 (1986).

[5] L.D. Skouras and C. Dedes, Phys. Rev. C **15**, 1873 (1977).

[6] A. Goswami and O. Nalcioglu, Phys. Lett. **26B**, 353 (1968).

[7] J. Vanhorenbeeck, P. Duhamel, P. Del Marmol, P. Fettweis, and K. Heyde, Nucl. Phys. **A408**, 265 (1983).

[8] H.A. Roth, S.E. Arnell, D. Foltescu, O. Skeppstedt, J. Blom-qvist, A. Nilsson, T. Kuroyanagi, S. Mitarai, and J. Nyberg, Phys. Rev. C **50**, 1330 (1994).

[9] W. Reviol, U. Garg, A. Aprahamian, M.P. Carpenter, B.F. Davis, D. Ye, R.V.F. Janssens, T.L. Khoo, T. Lauritsen, Y. Liang, S. Naguleswaran, and J.C. Walpe, Nucl. Phys. **A557**, 391c (1993).

[10] S.S. Ghugre and S.K. Datta, Phys. Rev. C **52**, 1881 (1995).

[11] S.S. Ghugre, S.B. Patel, M. Gupta, R.K. Bhowmik, and J.A. Sheikh, Phys. Rev. C **50**, 1346 (1994).

[12] J. Gizon, D. Jerrestam, A. Gizon, M. Jozsa, R. Bark, B. Fogel-berg, E. Ideguchi, W. Klamra, T. Lindblad, S. Mitarai, J. Ny-berg, M. Piiparinen, and G. Sletten, Z. Phys. A **345**, 335 (1993).

[13] R. Wyss (private communication).

[14] Ch. Winter, D.J. Blumenthal, P. Chowdhury, B. Crowell, P.J. Ennis, C.J. Gross, J. Heese, A. Junglaus, K.P. Lieb, D. Ru-dolph, M.A. Bentley, W. Gelletly, J. Simpson, J.L. Durell, and B.J. Varley, Nucl. Phys. **A535**, 137 (1991).

[15] I.Y. Lee, Nucl. Phys. **A520**, 641c (1990).

[16] S.S. Ghugre, B. Kharraja, U. Garg, M.P. Carpenter, B. Crow-ell, R.V.F. Janssens, T.L. Khoo, T. Lauritsen, D. Nisius, W. Mueller, W. Reviol, L.L. Riedinger, and R. Kaczarowski (un-published).

[17] D.C. Radford, I. Ahmad, R. Holzmann, R.V.F. Janssens, and T.L. Khoo, Nucl. Instrum. Methods Phys. Res. A **258**, 111 (1987).

[18] J.A. Kuehner, J.C. Waddington, and D. Prevost, *Proceedings of the International Conference on Nuclear Structure at High Angular Momentum*, Ottawa, 1992, edited by J.C. Waddington and D. Ward, Report No. AECL-10613, 1992 (unpublished), p. 413.

[19] D.C. Radford, Nucl. Instrum. Methods Phys. Res. A **361**, 297 (1995).

[20] G. Palameta and J.C. Waddington, Nucl. Instrum. Methods Phys. Res. A **234**, 476 (1985).

[21] B. Crowell, M.P. Carpenter, R.G. Henry, R.V.F. Janssens, T.L. Khoo, T. Lauritsen, and D. Nisius, Nucl. Instrum. Methods Phys. Res. A **355**, 575 (1995).

[22] S.S. Ghugre, S. Naguleswaran, R.K. Bhowmik, U. Garg, S.B. Patel, W. Reviol, and J.C. Walpe, Phys. Rev. C **51**, 2809 (1995).

[23] E.H. Du Marchie, Van Voorthuysen, M.J.A. DeVoigt, N. Blasi, and J.F.W. Jansen, Nucl. Phys. **A355**, 93 (1981).

[24] G.S. Samudra, K.D. Carnes, F.A. Rickey, P.C. Simms, and S. Zeghib, Phys. Rev. C **37**, 605 (1988).

[25] J.B. Ball, J.B. McGrory, and J.S. Larsen, Phys. Lett. **41B**, 581 (1972).

[26] B.A. Brown, A. Etchegoyen, W.D.M. Rae, and N.S. Godwin (unpublished).

[27] D.H. Gloeckner, Nucl. Phys. **A253**, 301 (1975).

[28] M.A. Deleplanque, J.C. Bacelar, E.M. Beck, R.M. Diamond, F.S. Stephens, J.E. Draper, Th. Dossing, and K. Neergaard, Phys. Lett. B **195**, 17 (1987).

[29] M.K. Kabadiyski, F. Cristancho, C.J. Gross, A. Jungclaus, K.P. Lieb, D. Rudolph, H. Grawe, J. Heese, K.-H. Maier, J. Eberth, S. Skoda, W.T. Chow, and E.K. Warburton, Z. Phys. A **343**, 165 (1992).

[30] M. Behar, A. Ferrero, A. Filevich, G. Garcia Bermudez, and M.A.J. Mariscotti, Nucl. Phys. **A373**, 483 (1982).

[31] B. Kharraja, S.S. Ghugre, U. Garg, M.P. Carpenter, B. Crow-ell, S. Fischer, R.V.F. Janssens, T.L. Khoo, T. Lauritsen, D. Nisius, W. Mueller, W. Reviol, L.L. Riedinger, I.M. Govil, R. Kaczarowski, and E. Ruchowska (unpublished).

[32] C. Baktash, in *High Angular Momentum Properties of Nuclei*, edited by N.R. Johnson (Harwood Academic, New York, 1983), p. 207.